Reaction-driven oscillating viscous fingering

Cite as: Chaos **29**, 043115 (2019); https://doi.org/10.1063/1.5089028
Submitted: 16 January 2019 . Accepted: 28 March 2019 . Published Online: 19 April 2019

C. Rana, and A. De Wit

Reaction-driven oscillating viscous fingering

Cite as: Chaos **29**, 043115 (2019); doi: 10.1063/1.5089028
Submitted: 16 January 2019 · Accepted: 28 March 2019 ·
Published Online: 19 April 2019

View Online Export Citation CrossMark

C. Rana and A. De Wit[a)]

AFFILIATIONS

Nonlinear Physical Chemistry Unit, Université libre de Bruxelles (ULB), 1050 Brussels, Belgium

Note: This paper is part of the Focus Issue, "Nonlinear Chemical Dynamics and Its Interdisciplinary Impact: Dedicated to Ken Showalter on the Occasion of his 70th Birthday."
[a)]**Electronic mail:** adewit@ulb.ac.be

ABSTRACT

Localized oscillations can develop thanks to the interplay of reaction and diffusion processes when two reactants A and B of an oscillating reaction are placed in contact, meet by diffusion, and react. We study numerically the properties of such an $A + B \rightarrow$ oscillator configuration using the Brusselator model. The influence of a hydrodynamic viscous fingering instability on localized concentration oscillations is next analyzed when the oscillating chemical reaction changes the viscosity of the solutions involved. Nonlinear simulations of the related reaction–diffusion–convection equations with the fluid viscosity varying with the concentration of an intermediate oscillatory species show an active coupling between the oscillatory kinetics and the viscously driven instability. The periodic oscillations in the concentration of the intermediate species induce localized changes in the viscosity, which in turn can affect the fingering instability. We show that the oscillating kinetics can also trigger viscous fingering in an initially viscously stable displacement, while localized changes in the viscosity profile can induce oscillations in an initially nonoscillating reactive system.

Pattern formation and complex spatiotemporal dynamics are ubiquitously observed in nature, including, in particular, in hydrodynamic and chemical systems. In hydrodynamics, convective instabilities at interfaces can be due to gradients in density, viscosity, or surface tension, for instance. As an example, viscous fingering (VF) occurs at an interface between two miscible fluids when the less viscous fluid displaces the more viscous one. It induces deformation of the interface in fingerlike forms and increases mixing between the two solutions. In chemical systems, nonlinear feedback in the kinetics can be responsible for oscillations of concentrations and complex spatiotemporal dynamics in spatially extended systems. We explore here the interplay between chemical oscillations and viscous fingering showing that the two mechanisms of instability can affect one another, but also, more strikingly, that concentration oscillations can trigger fingering, while viscous gradients can induce oscillations in situations that are stable in the absence of chemohydrodynamic coupling.

I. INTRODUCTION

The interplay between chemical reactions and hydrodynamics at the interface between two miscible solutions of reactants has attracted increasing interest over the past few decades due to its applications in environmental issues as well as in petroleum and chemical engineering.[1] In chemohydrodynamics, pioneering work has been developed by Showalter and colleagues in the 1990s, showing that density gradients across autocatalytic fronts can deform and accelerate the fronts.[2–5] The self-organized reaction zone between reactants and products of an autocatalytic reaction travels then in space and provides the miscible interface across which convective flows can develop due to density differences. In the case of viscosity gradients triggering a viscous fingering instability, bistable reactions have been shown to be able to produce droplets detaching from growing viscous fingers.[6]

For simple bimolecular $A + B \rightarrow C$ reactions, chemical reaction–diffusion (RD) fronts can develop when a solution of A is put in contact with a solution of B.[7] Across such fronts, convective currents can develop due to density differences in the gravity field or surface tension gradients.[8] The interplay between viscous fingering and such $A + B \rightarrow C$ fronts has also been largely studied both experimentally[9–11] and theoretically[12,13] when the chemical reaction influences the viscosity gradient. Similarly, aggregation of nanoparticles on the porous matrix can result in variations of the viscosity gradient and can thus play a crucial role in the control of viscous fingering.[14,15]

Recently, special attention has been put on understanding how localized temporal oscillations of chemical concentrations can also actively couple to hydrodynamic flows to produce pulsatile flows.[16–18] Localized oscillations[19] or stationary Turing patterns[20,21] can be obtained in autocatalytic reactions around A + B → oscillator fronts when putting in contact two zones containing separate reactants A and B of an oscillatory reaction.[17,18,22,23] From the theoretical point of view, it has been shown that localized oscillations and Turing structures can interact with buoyancy-driven flows when the reactants A and B of the oscillatory Brusselator model are initially separated, meet by diffusion, and produce the intermediate X and Y species locally, which changes the density.[18] Experimentally, interplay between the oscillating Belousov–Zhabotinsky (BZ) reaction and buoyancy-driven motions has been analyzed when two subsets of the reactants are put in contact along a horizontal line in the gravity field.[16,24]

With regard to the viscous fingering instability occurring when a less viscous solution displaces a more viscous one in a porous medium or Hele-Shaw cell (two glass plates separated by a thin gap), interplay with an oscillating reaction can be obtained only if the reaction induces sufficient viscosity changes. Using pH-sensitive polymers, Escala *et al.* have recently obtained a clock type change of viscosity thanks to a coupling with a pH clock reaction.[25] On this basis, they have further shown that this reaction-driven viscosity change is able to destabilize the otherwise hydrodynamically stable displacement of a less viscous aqueous reactive solution by a more viscous solution of a pH-sensitive polymer.[26] This experimental result suggests that more complex dynamics could be obtained if viscous fingering can be coupled to temporal oscillations of pH.

The goal of this article is to move a step further and probe the viscous destabilization of an initially stable system when an $A + B \rightarrow$ oscillator front induces localized periodic variations of viscosity. To do so, we explore numerically the interplay between temporal oscillations of concentrations in the Brusselator model and viscous fingering when the viscosity of the solution varies with the concentration of the Y intermediate species. We show that an oscillating localized pattern can be sustained, influenced, and induced by the viscous fingering instability thanks to an interplay of chemistry and hydrodynamics. In particular, the striking prediction of our study is that, if the chemical system and the hydrodynamic displacement are stable on their own, a chemohydrodynamic instability can arise due to the coupling of the autocatalytic kinetics with viscosity gradients. Indeed, we show that subcritical oscillations can be fired by viscous fingers, while local viscosity gradients induced by oscillations can trigger local fingering in otherwise stable configurations.

The outline of the paper is as follows: In Sec. II, we describe the reaction–diffusion–convection model with Brusselator kinetics in an A + B → oscillator configuration and viscosity changes coupled to the concentration of the Y intermediate species. A discussion of the numerical approach with stability and discretization considerations is given next. In Sec. III, we discuss the numerical simulation results evidencing the coupled influence of oscillating patterns with the convective viscous fingering instability. The paper is concluded in Sec. IV.

II. CHEMOHYDRODYNAMIC MODEL

Our model system is a two-dimensional porous medium of length L_x and width L_y filled with a solution of the reactant A in concentration A_0 with viscosity μ_A. At a given time, a finite slice of width W containing both reactants A and B in concentration A_0 and B_0, respectively, and of viscosity μ_s is injected in the system (Fig. 1) and displaced at a constant speed U along the x axis by the solution of A. The reactants A and B are then involved in the nonlinear kinetics of the irreversible Brusselator model given by[19,27–35]

$$\begin{aligned} A &\xrightarrow{k_1} X, \\ B + X &\xrightarrow{k_2} Y + D, \\ 2X + Y &\xrightarrow{k_3} 3X, \\ X &\xrightarrow{k_4} E. \end{aligned} \tag{1}$$

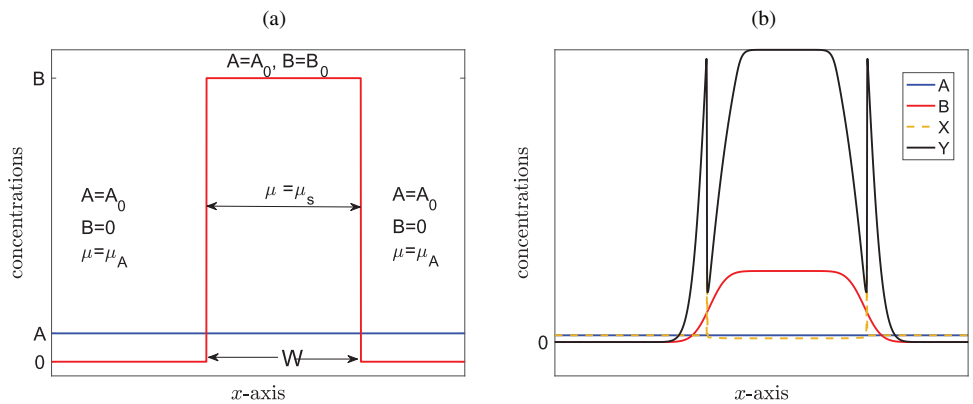

FIG. 1. Schematic of the spatial concentration profiles of (a) the Brusselator chemical reactants A and B at time $t = 0$ and (b) reactants A and B and intermediate species X and Y some time after oscillations have started.

Here, $\{k_i, i = 1, 4\}$ represent the set of rate constants, and X and Y are the intermediate oscillating species, respectively. The Brusselator model has been used previously to obtain localized oscillations and Turing patterns within gradients of concentration of reactants.[18,19,22,31–35]

Here, specifically, the initial concentrations of the various reactant species in the configuration described in Fig. 1 is

$$(A, X, Y)(x, y, t = 0) = (A_0, 0, 0) \quad \forall x, y, \tag{2}$$

$$B(x, y, t = 0) = \begin{cases} B_0 & \text{for } x \in W, \\ 0 & \text{elsewhere,} \end{cases} \quad \forall y. \tag{3}$$

A. Reaction–diffusion–convection equations

Upon diffusion and reaction between the two reactants A and B, nonlinear dynamics of the intermediate species X and Y start to develop in the localized reaction zone of width W [see Fig. 1(b)]. Assuming that the viscosity of the medium is a function of the concentration of species Y and that the flow is governed by Darcy's law, the two-dimensional chemohydrodynamics of the system is described by the following reaction–diffusion–convection equations:

$$\underline{\nabla} \cdot \underline{u} = 0, \tag{4}$$

$$\underline{\nabla} p = -\frac{\mu(Y)}{\kappa} \underline{u}, \tag{5}$$

$$\frac{\partial A}{\partial t} + \underline{u} \cdot \underline{\nabla} A = -k_1 A + D_A \nabla^2 A, \tag{6}$$

$$\frac{\partial B}{\partial t} + \underline{u} \cdot \underline{\nabla} B = -k_2 B X + D_B \nabla^2 B, \tag{7}$$

$$\frac{\partial X}{\partial t} + \underline{u} \cdot \underline{\nabla} X = k_1 A - k_2 B X + k_3 X^2 Y - k_4 X + D_X \nabla^2 X, \tag{8}$$

$$\frac{\partial Y}{\partial t} + \underline{u} \cdot \underline{\nabla} Y = k_2 B X - k_3 X^2 Y + D_Y \nabla^2 Y. \tag{9}$$

Here, $\underline{u} = (u, v)$ is the velocity field and D_J is the molecular diffusion coefficient of species J, which is supposed to be constant. We assume that there are no buoyancy effects and that the dynamic viscosity μ varies exponentially with the concentration of Y as[6]

$$\mu(Y) = \mu_A e^{R \frac{Y}{Y_c}}, \tag{10}$$

where $R = \ln \frac{\mu_s}{\mu_A}$ is the log-mobility ratio quantifying the ratio between the viscosity μ_s of the sample when $Y = Y_c$ and the viscosity μ_A of the displacing solution of A, where Y_c is a reference concentration of Y. The equations are nondimensionalized using the following scaling:

$$\tilde{u} = u/U, \quad (\tilde{x}, \tilde{y}) = (x/(U/k_4), y/(U/k_4)), \quad \tilde{t} = k_4 t,$$

$$\tilde{D}_J = D_J/(U^2/k_4), \quad \tilde{A} = A/A_c, \quad \tilde{B} = B/B_c,$$

$$\tilde{X} = X/X_c, \quad \tilde{Y} = Y/Y_c,$$

where

$$X_c = Y_c = \sqrt{\frac{k_4}{k_3}}, \quad A_c = \frac{k_4}{k_1}\sqrt{\frac{k_4}{k_3}}, \quad B_c = k_4 k_2.$$

The resulting nondimensional governing equations in a frame of reference moving with the injection velocity are (after dropping the tildes)

$$\underline{\nabla} \cdot \underline{u} = 0, \tag{11}$$

$$\underline{\nabla} p = -\mu(Y)(\underline{u} + \underline{e}_x), \tag{12}$$

$$\frac{\partial A}{\partial t} + \underline{u} \cdot \underline{\nabla} A = -k_A A + D_A \nabla^2 A, \tag{13}$$

$$\frac{\partial B}{\partial t} + \underline{u} \cdot \underline{\nabla} B = -k_B B X + D_B \nabla^2 B, \tag{14}$$

$$\frac{\partial X}{\partial t} + \underline{u} \cdot \underline{\nabla} X = A - (B + 1)X + X^2 Y + D_X \nabla^2 X, \tag{15}$$

$$\frac{\partial Y}{\partial t} + \underline{u} \cdot \underline{\nabla} Y = B X - X^2 Y + D_Y \nabla^2 Y, \tag{16}$$

$$\mu = e^{RY}, \tag{17}$$

where $k_A = k_1/k_4$, $k_B = k_2/\sqrt{k_3 k_4}$, and $\underline{e}_x$ is the unit vector along the x-direction. In the remainder of the article, we assume that both reactants A and B have the same diffusivity and fix $D_A = D_B = 1$. In batch conditions such that A and B are kept at constant concentrations A_0 and B_0 and no convective instability can occur, this model admits a homogeneous steady-state solution $X_s = A_0$, $Y_s = B_0/A_0$, which is unstable toward temporal oscillations of the intermediate species X and Y when $B_0 > B_c = 1 + A_0^2$. In the absence of reactions but provided some Y species is present in the sample, VF can occur as soon as $R \neq 0$. Here, we take $R > 0$ such that VF develops at the back left part of the sample where the less viscous solution of A displaces the more viscous sample.

In order to analyze numerically the localization of such oscillations for the initial conditions (2) and (3) and their coupling with viscous fingering, we use a stream-function formulation by introducing the stream function Ψ defined as $(u, v) = (\partial\Psi/\partial y, -\partial\Psi/\partial x)$. The governing equations (11)–(17) reduce to

$$\nabla^2 \Psi = -R(\Psi_x Y_x + \Psi_y Y_y + Y_y), \tag{18}$$

$$A_t + \Psi_y A_x - \Psi_x A_y = -k_A A + \nabla^2 A, \tag{19}$$

$$B_t + \Psi_y B_x - \Psi_x B_y = -k_B B X + \nabla^2 B, \tag{20}$$

$$X_t + \Psi_y X_x - \Psi_x X_y = A - (B + 1)X + X^2 Y + D_X \nabla^2 X, \tag{21}$$

$$Y_t + \Psi_y Y_x - \Psi_x Y_y = B X - X^2 Y + D_Y \nabla^2 Y, \tag{22}$$

where subscripts indicate a derivative with regard to the subscript variable. It is expected that this model will give localized oscillations in the sample when $B_0 > 1 + A_0^2$ and VF at the left part of the sample[36,37] when $R > 0$.

B. Numerical approach

Equations (18)–(22) are solved numerically using Fourier pseudospectral techniques.[38] In this technique, the variables A, B, Y, X, and Ψ are transformed into Fourier space as

$$I(x, y, t) = \sum_p \sum_r \hat{I}_{p,r}(t) e^{i(k_p x + k_r y)}, \tag{23}$$

where $i^2 = -1$, $I(x, y, t)$ is the variable in real space while $\hat{I}$ are the Fourier coefficients of I calculated at the discretized collocation points, and k_p and k_r are the wave numbers of the Fourier modes. The Fourier discretization is uniform in space and is truncated at $p = 0$ and $p = M - 1$, $r = 0$ and $r = N - 1$, where M and N are the number of grid points in the x and y directions, respectively. The nonlinear and variable coefficient terms are calculated in real physical space. The transformation between the real and the Fourier space is done by using fast Fourier transformation with the order of complexity $\mathbf{N}\log_2\mathbf{N}$, where $\mathbf{N} = M \times N$.

To apply the spectral technique, nonlinear terms are defined in terms of Fourier coefficients as

$$N_Y(x,y,t) = \frac{\partial \Psi}{\partial x}\frac{\partial Y}{\partial x} + \frac{\partial \Psi}{\partial y}\frac{\partial Y}{\partial y} = \sum_p \sum_r \hat{N}_{Y_{p,r}}(t) e^{i(k_p x + k_r y)}, \quad (24)$$

$$J_A(x,y,t) = \frac{\partial \Psi}{\partial y}\frac{\partial A}{\partial x} - \frac{\partial \Psi}{\partial x}\frac{\partial A}{\partial y} + k_A A = \sum_p \sum_r \hat{J}_{A_{p,r}}(t) e^{i(k_p x + k_r y)}, \quad (25)$$

$$J_B(x,y,t) = \frac{\partial \Psi}{\partial y}\frac{\partial B}{\partial x} - \frac{\partial \Psi}{\partial x}\frac{\partial B}{\partial y} + k_B B X = \sum_p \sum_r \hat{J}_{B_{p,r}}(t) e^{i(k_p x + k_r y)}, \quad (26)$$

$$J_X(x,y,t) = \frac{\partial \Psi}{\partial y}\frac{\partial X}{\partial x} - \frac{\partial \Psi}{\partial x}\frac{\partial X}{\partial y} - A + (B+1)X - X^2 Y = \sum_p \sum_r \hat{J}_{X_{p,r}}(t) e^{i(k_p x + k_r y)}, \quad (27)$$

$$J_Y(x,y,t) = \frac{\partial \Psi}{\partial y}\frac{\partial Y}{\partial x} - \frac{\partial \Psi}{\partial x}\frac{\partial Y}{\partial y} - BX + X^2 Y = \sum_p \sum_r \hat{J}_{Y_{p,r}}(t) e^{i(k_p x + k_r y)}. \quad (28)$$

With the above representation, the equations become in Fourier space a system of algebraic differential equations:

$$\hat{\Psi}_{p,r} = R(\hat{N}_{Y_{p,r}} + ik_r \hat{Y}_{p,r})/({k_p}^2 + {k_r}^2), \quad (29)$$

$$\frac{d\hat{A}_{p,r}}{dt} = -\hat{J}_{A_{p,r}} - (k_p^2 + k_r^2)\hat{A}_{p,r}, \quad (30)$$

$$\frac{d\hat{B}_{p,r}}{dt} = -\hat{J}_{B_{p,r}} - (k_p^2 + k_r^2)\hat{B}_{p,r}, \quad (31)$$

$$\frac{d\hat{X}_{p,r}}{dt} = -\hat{J}_{X_{p,r}} - D_X(k_p^2 + k_r^2)\hat{X}_{p,r}, \quad (32)$$

$$\frac{d\hat{Y}_{p,r}}{dt} = -\hat{J}_{Y_{p,r}} - D_Y(k_p^2 + k_r^2)\hat{Y}_{p,r}. \quad (33)$$

The terms $\hat{N}_Y, \hat{J}_A, \hat{J}_B, \hat{J}_X$, and $\hat{J}_Y$ are evaluated by transforming variables $\hat{A}, \hat{B}, \hat{\Psi}, \hat{X}$, and $\hat{Y}$ to real physical space, computing all the terms having nonlinear and variable coefficients in the real physical space and then transforming back to Fourier space. The time-stepping scheme is a predictor–corrector method with second order Adams–Bashforth scheme corrected by using a trapezoidal rule.[36,39]

We investigate numerically the spatiotemporal dynamics of the Brusselator model with a focus on the influence of viscous fingering. The robustness of the numerical scheme is established by obtaining the stable state configuration X_s, Y_s for $B_0 < B_c$ and $R = 0$ as well as classical VF of a localized sample[36,37] if Y is kept locally constant in the sample and $R > 0$. For computation purposes, the nondimensional length and width of the domain are $L = k_4 L_x/U$ and $L' = k_4 L_y/U$, respectively, with the nondimensional initial length of the sample zone being $W_s = k_4 W/U = 764$. To apply the Fourier pseudospectral method, periodic boundary conditions are employed along the longitudinal and transverse direction.[36,39] Our simulations are performed on a rectangular domain discretized using a lattice of 2048 × 256 grid points with a spatial step size of 0.5 and a time step of 0.01. We fix the values $D_X = D_Y = 0.3$ and $k_A = k_B = 10^{-6}$. The small values of k_A and k_B allow one to focus on oscillations before A and B are all consumed by the first steps of the Brusselator kinetics (1). Taking equal diffusion coefficients for X and Y allows to avoid a Turing instability. Keeping $A_0 = 0.1$ throughout such that $B_c = 1.01$, we vary B_0 and R such that the computed solution eventually settles in one of the following states: spatially homogeneous steady state, oscillating patterns or aperiodic oscillations, and viscous fingering. The initial width W_s of the sample is a crucial parameter, which determines the spatiotemporal morphology of the oscillating patterns. If the width of the region is too small, then the oscillations die out before the onset of viscous fingering. Therefore, the width of the sample is taken here large enough for the oscillations to be sustained on the time scale needed for viscous fingering to operate.

III. RESULTS AND DISCUSSIONS

The chemohydrodynamic patterns studied here can be analyzed by following the evolution of the two-dimensional (2D) $X(x, y, t)$ and $Y(x, y, t)$ concentration fields of the oscillating intermediate species. At successive times, these 2D concentration fields can be spatially averaged along the transverse y coordinate to yield one-dimensional (1D) transversely averaged profiles, i.e., $\bar{X}, \bar{Y}$ defined as[40]

$$\bar{X}(x,t) = \frac{1}{L'}\int_0^{L'} X(x,y,t)dy, \quad (34)$$

$$\bar{Y}(x,t) = \frac{1}{L'}\int_0^{L'} Y(x,y,t)dy. \quad (35)$$

The parameter space is classified on the basis of the RD dynamics controlled here by the initial reactant concentration A_0, B_0 and by the contribution of Y to the viscous fingering instability dynamics controlled by the log-mobility ratio R. We begin with the reference case $R = 0$ for which no viscous fingering instability can develop as the displaced sample has then the same viscosity as the displacing solution of A. This reference oscillating situation is instructive to next gradually characterize the oscillating pattern in the presence of viscous fingering instability obtained when $R \neq 0$.

A. Localized oscillations in the absence of VF ($R = 0$)

In the absence of any viscous fingering ($R = 0$), the concentration of the intermediate species X and Y evolves within the sample toward the steady state value $(X_s, Y_s) = (A_0, B_0/A_0)$ if $B_0 < B_c = 1 + A_0^2 = 1.01$ [Figs. 2(a) and 2(b)]. On the contrary, for $B_0 > B_c$,

the steady state becomes unstable and the system features localized periodic oscillations of X and Y within the sample [Figs. 2(c) and 2(d)]. These temporal oscillations can be best appreciated by looking at the transversely averaged concentration profile $\bar{Y}(x_c, t)$ at three different fixed points x_c within the finite reaction zone (Fig. 3). The x_c points are chosen at positions that correspond to $0.1W_s$, $0.5W_s$, and $0.9W_s$, respectively, to analyze the dynamics at the left, middle, and right of the sample, respectively. We see that the central point maintains regular oscillations with a fixed amplitude, while the lateral points see a decrease in time of their amplitude because of diffusion of B within the sea of A. The resulting local decrease of B at the edge of the sample ultimately leads to fading of the oscillations in time at the boundaries of the sample. In the absence of VF, the spatiotemporal dynamics at the left and right of the sample feature symmetric behaviors (Fig. 3). The larger the sample, the longer regular oscillations are maintained in its central part. Here, the initial sample width W_s is always taken large enough for the interplay between chemistry and hydrodynamics to occur before diffusive fading out of oscillations in its central part.

As it is the location where oscillations are maintained for the longest time, the center point of the reaction zone is used to measure the amplitude of the oscillations Y_{amp}. Figure 4(a) shows the temporal evolution of the transverse average concentration $\bar{Y}$ at this center location for different values of B_0, while the related amplitude of the oscillations, Y_{amp}, is plotted as a function of B_0 in Fig. 4(b). Clearly, Y_{amp} increases as B_0 increases above B_c. For $B_0 = B_c$, tiny little modulations of concentrations are observed, while the amplitude sharply increases as soon as $B_0 > B_c$ because of the small value of A_0 used here.

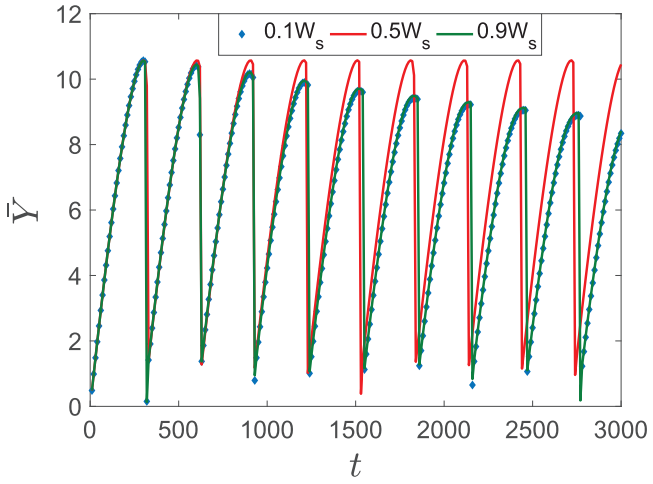

FIG. 3. Temporal evolution of the transverse average concentration $\bar{Y}(x_c, t)$ for $B_0 = 1.04$, $R = 0$ at different fixed positions, x_c, inside the sample, i.e., $x_c = 0.1W_s$, $0.5W_s$, and $0.9W_s$.

These simulations show that localized temporal oscillations can be controlled by the initial concentration of B within the sample. Next, we examine how these oscillations couple to viscous fingering when the viscosity contrast between the displacing fluid A and the sample is nonzero.

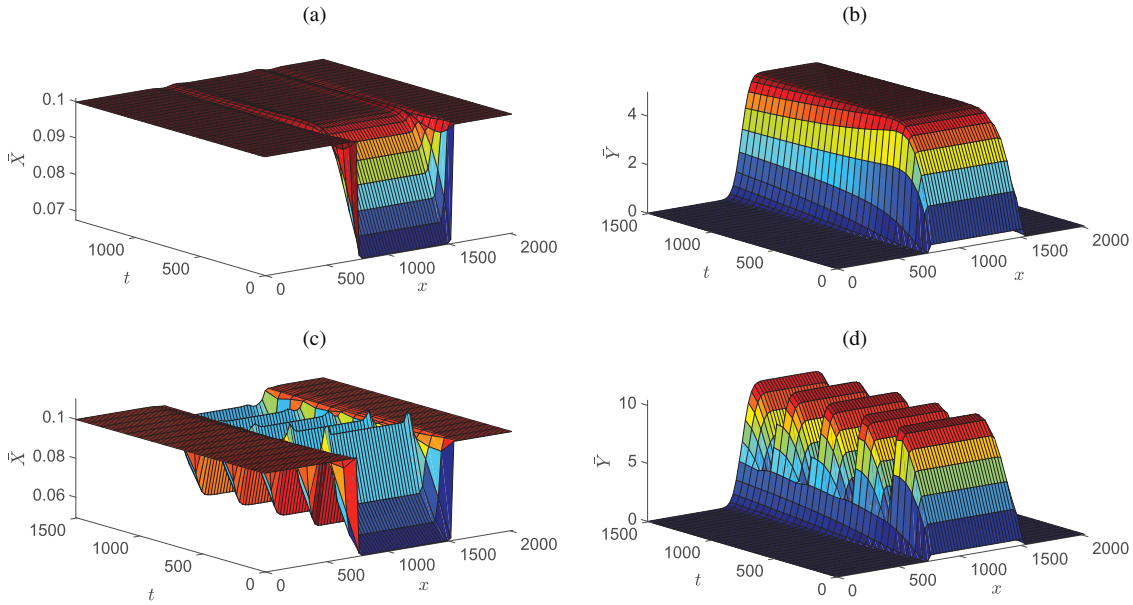

FIG. 2. Temporal evolution of the transversely averaged profiles of the intermediate species X and Y. In the nonoscillating case shown in the first line for $B_0 = 0.5$, X evolves to the steady state $X_s = A_0$ (a), while Y asymptotes to $Y_s = B_0/A_0$ (b) within the sample. For $B_0 = 1.04$, i.e., for $B_0 > 1 + A_0^2$, the variables X (c) and Y (d) start to oscillate locally in the sample.

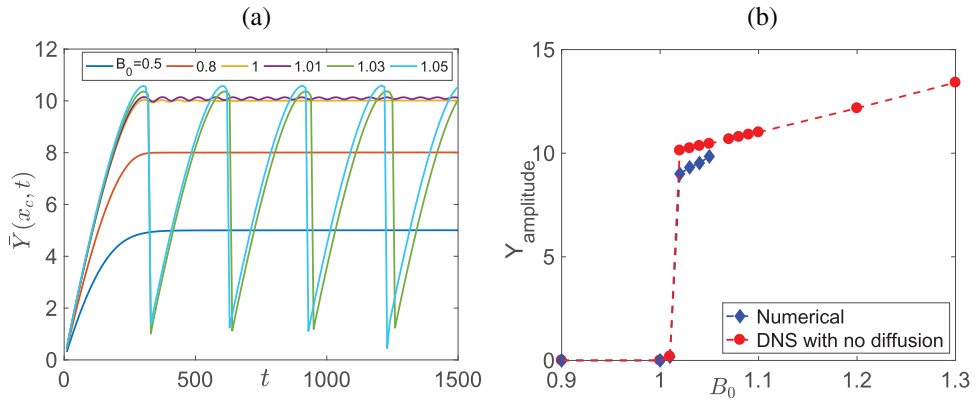

FIG. 4. (a) Temporal evolution of the transverse averaged concentration $\bar{Y}$ for different values of B_0 at the fixed position $x_c = 0.5W_s$ for $R = 0$. (b) Amplitude of the oscillations of the Y species as a function of B_0 computed either by direct numerical solution (DNS) of the Brusselator kinetics with no diffusion or at the central part of the sample.

B. Oscillating viscous fingering ($R > 0$)

When $R > 0$, the viscous fingering instability is triggered here at the rear, left part of the sample[36,37] where the less viscous solution of A with viscosity μ_A displaces the more viscous sample of viscosity μ_s. The 2D concentration field of species Y is compared in Fig. 5 for both nonoscillating ($B_0 < B_c$) and oscillating ($B_0 > B_c$) cases at $R = 0.2$ and 0.25. In the absence of oscillations, we see in Figs. 5(a) and 5(c) the classical fingering deformation of the rear interface where the viscosity increases along the flow direction. Within the sample, the concentration of X and Y remains constant and equal to their steady-state values X_s and Y_s, while they dilute out by diffusion at the right frontal interface where the viscous gradient is stable. In the oscillating case [Figs. 5(b) and 5(d)], the VF instability is observed to interplay with the oscillating pattern. The fingers still develop at the back of the sample; however, they appear earlier, while later on, fingering is

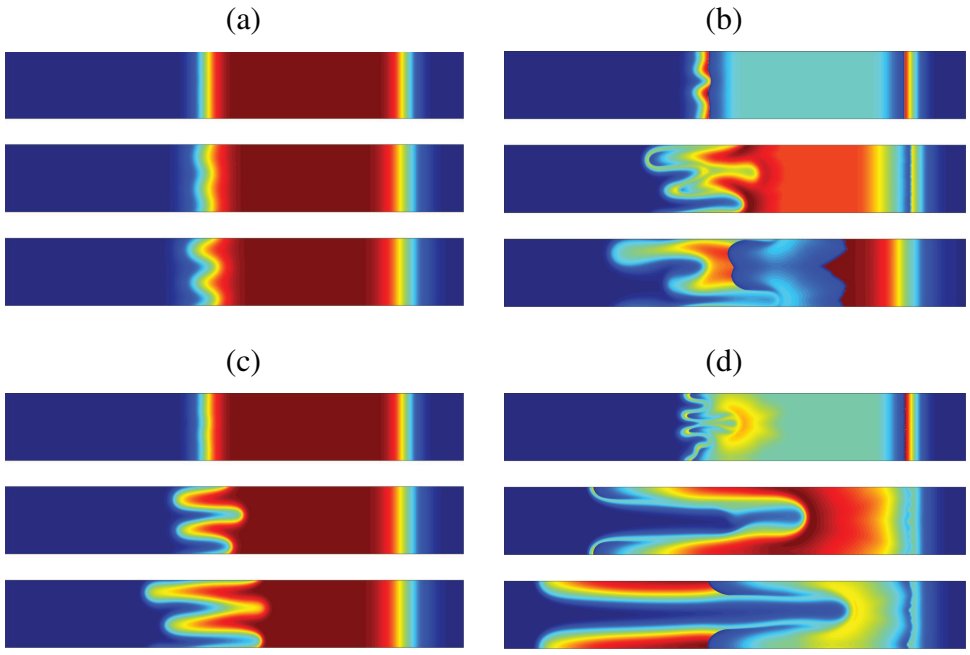

FIG. 5. Concentration fields of Y at three successive times $t = 1000, 2000$, and 2500 from top to bottom within a panel comparing viscous fingering in the nonoscillating case when $B = 0.5$ in the left column with the corresponding oscillating case at $B = 1.02$ in the right column for $R = 0.2$ [(a) and (b)] and $R = 0.25$ [(c) and (d)].

more intense leading to a more extended fingered zone. Within the sample, the concentration of Y oscillates in time; however, the oscillations become progressively spatially desynchronized because of the fingering. This is a clear example of a chemohydrodynamic structure in which the final pattern combines the properties of an oscillating reaction and of a viscous fingering instability. Let us further analyze the impact of oscillations on fingering and vice versa.

1. Influence of oscillations on VF

An important influence of the oscillations on fingering is to decrease the onset time of the hydrodynamic instability. For instance, in Fig. 5(a), the onset time of nonoscillating fingering for $R = 0.2$ is around $t = 2000$, whereas for the equivalent oscillatory case, fingering is observed before $t = 1000$ as seen in Fig. 5(b). The rationale behind the earlier onset of VF for the oscillating case is the fact that the oscillations in the concentration of Y induce a pulsating behavior of viscosity. These oscillations induce spatially traveling waves [see Fig. 6(a)] in which, locally, steeper viscosity gradients are obtained. This increases the viscous destabilization, inducing an earlier appearance of the fingers and a smaller wavelength. The extent of the fingered zone is also longer in the presence of oscillations as seen in Fig. 7, featuring the temporal evolution of the mixing length L of the concentration of Y calculated as the length of the interval in which the transverse averaged concentration $\bar{Y}(x,t) > 0.001$. The oscillating cases show a significant increase in mixing length in comparison with the nonoscillating cases. Thus, earlier triggering of convection, an increased number of fingers, and a larger mixing zone are some of the common features of VF in the presence of temporal oscillations of viscosity triggered by an oscillatory kinetics.

2. Influence of VF on oscillations

If fingering is affected by oscillations, the reverse is also true: typically, the local amplitude of the oscillations is modified in the presence of VF. Indeed, more intense mixing induced by the convective instability dilutes both the reactant B and the intermediate species X and Y of the oscillator. As a consequence, the oscillations are more quickly damped in the presence of VF and the larger R, i.e., the more intense the fingering, the quicker this effect. To see this, we plot in Fig. 6(b) the transverse average concentration $\bar{Y}$ as a function of time at the center position of the reaction zone. As explained in Fig. 4, for $R = 0$, the oscillations of species Y maintain a quite constant period and amplitude for the time scanned. For $R = 0.2$ and mild fingering, the oscillations start to show a dephasing and a small decrease in amplitude [Fig. 6(b)]. On further increasing R to 0.25, the dephasing occurs earlier with a significant decrease in the amplitude in comparison with $R = 0$. Thus, VF results in dampening of the chemical oscillations and this dampening is accelerated with

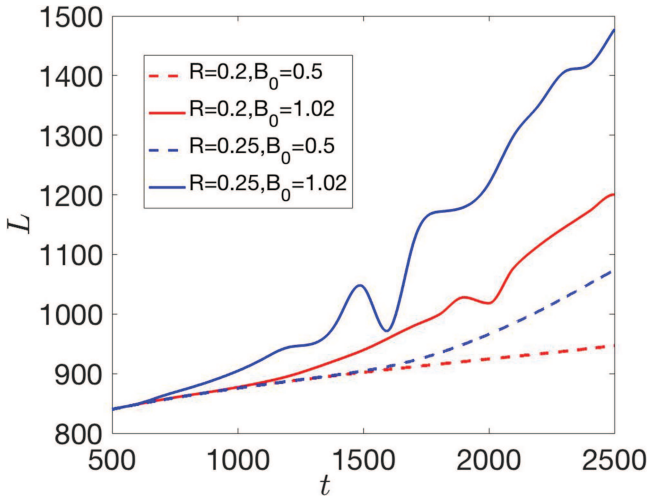

FIG. 7. Temporal evolution of the mixing length L for oscillating ($B = 1.02$, full curves) and nonoscillating ($B_0 = 0.5$, dashed curves) systems with $R = 0.2$ (red) and $R = 0.25$ (blue).

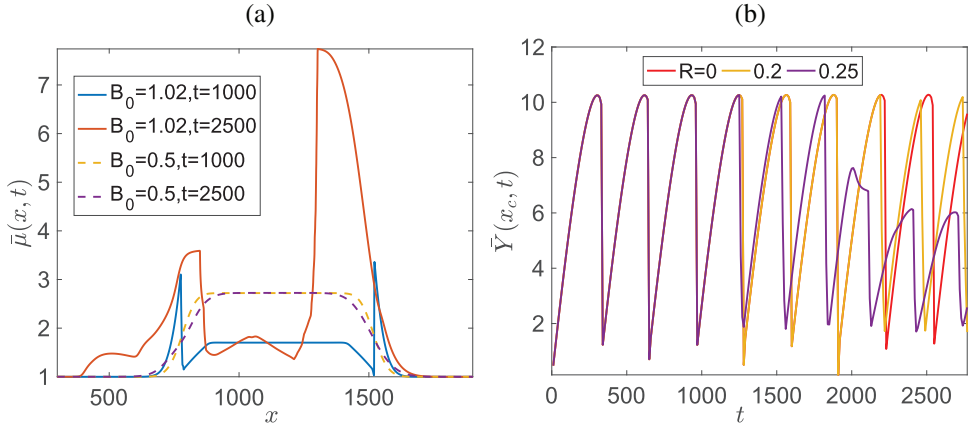

FIG. 6. (a) Transverse averaged viscosity profiles $\bar{\mu}$ for oscillating (solid curves) and nonoscillating (dashed curves) configurations at times $t = 1000$ and $t = 2500$ for $R = 0.2$, illustrating the pulsatile changes of viscosity with larger viscosity gradients for the oscillating case. (b) Transverse averaged concentration $\bar{Y}(x_c, t)$ at the fixed central position $x_c = 0.5W_s$ for different values of R and $B_0 = 1.02$.

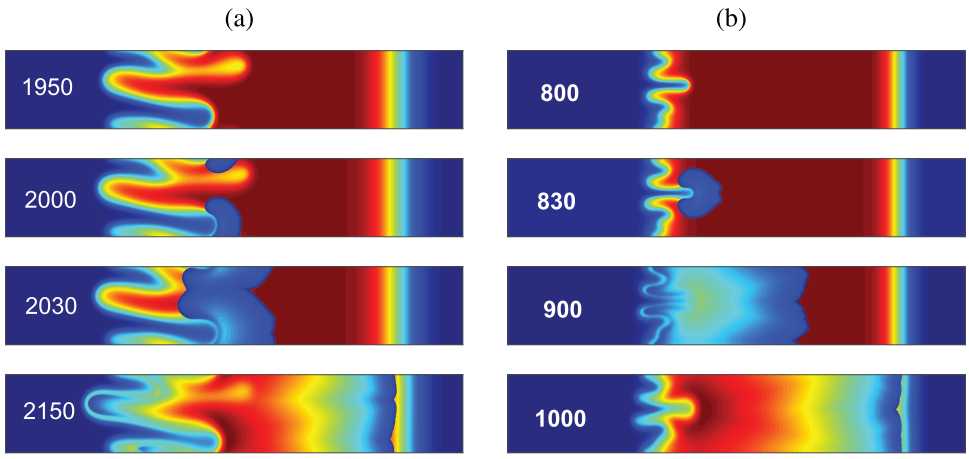

FIG. 8. Evolution of the 2D concentration field of Y for $B_0 = 1.00$ and (a) $R = 0.15$ and (b) $R = 0.20$ at the time indicated in the panel. As $B < B_c$, the central part of the sample does not oscillate. Oscillations are triggered in the valley where a finger depleted in B (in blue here) protrudes in the zone rich in B (in red).

an increase in the viscosity ratio R between the reactants A and B solutions.

The next question to be answered is whether VF could trigger oscillations in an otherwise nonoscillating system. If yes, then under what conditions can this be achieved and how do the induced oscillations get affected by a change in the viscosity contrast? As a corollary, we also seek to understand whether oscillations can destabilize a hydrodynamic stable displacement.

C. Oscillations induced by VF

We recall that, as $A = 0.1$ everywhere here, the threshold for oscillations is $B_c = 1.01$. Thus, when $B_0 < B_c$, no oscillations are expected in the system. We find, however, that, in the presence of viscous fingering, subcritical oscillations can be triggered locally. This is shown in Fig. 8(a) for $B_0 = 1.00 < B_c$ and $R = 0.15$. At the beginning, the system is stable toward oscillations and VF develops at the

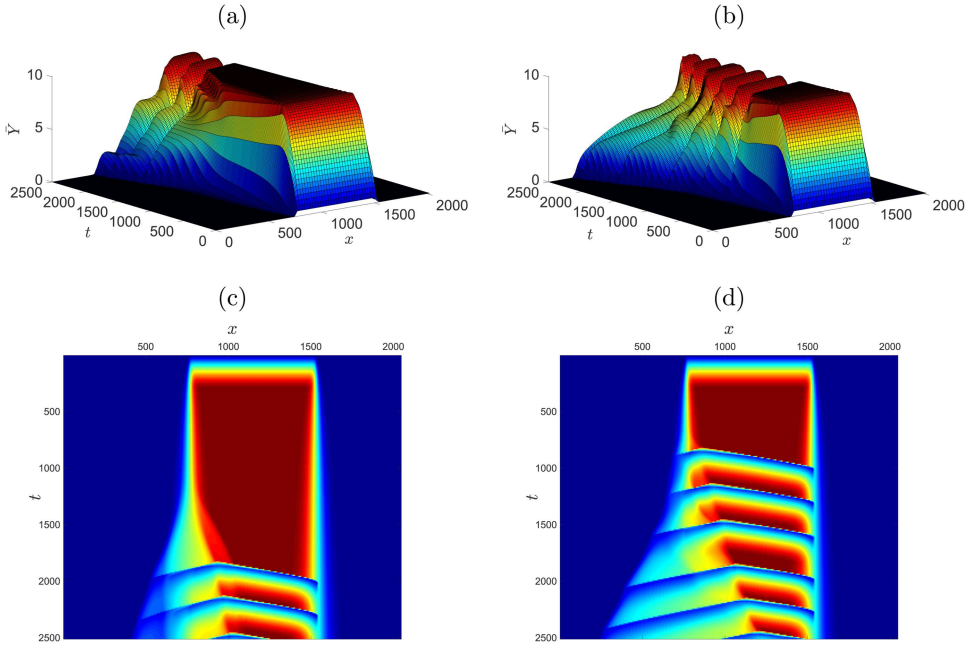

FIG. 9. (a) The transversed averaged evolution profile for Y with $B_0 = 1.00$ for (a) $R = 0.15$ and (b) $R = 0.2$ with the corresponding space-time plots in (c) and (d).

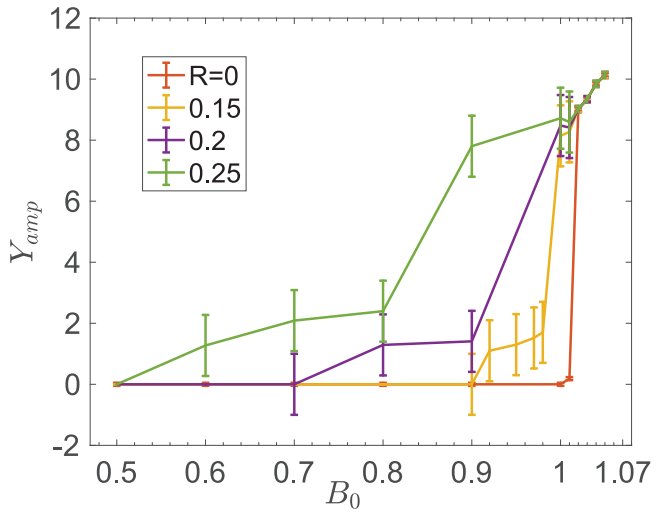

FIG. 10. Amplitude of oscillations as a function of B_0, for different values of R.

rear, left part of the sample in which Y equals its steady-state value. However, at some point, we observe that an oscillation starts at the trough of a finger, at the location where the blue finger of A, poor in B, X, and Y enters the sample rich in these three species. This local oscillation next triggers a wave that propagates across the sample. A second oscillation starts then again at the valley of the same finger generating a second wave. After the passage of this wave, the sample restores the constant steady state concentration in the middle of the sample.

This dynamics can be appreciated also in Fig. 8(b) where similar fingering-induced subcritical oscillations are obtained for a larger $R = 0.20$. Here, VF occurs sooner, is more intense, and has a smaller wavelength because R is larger. Oscillations and the related waves are also triggered at the tip of the fingers of the displacing fluid invading the sample. The oscillations are not fired at regular intervals as this occurs only when good conditions are met within invading fingers. Therefore, we see sometimes that oscillations disappear and the steady state is restored within the sample once classical merging of fingers leads to homogenization. Oscillations are triggered back only much later again, once a single finger is formed allowing for the blue finger to protrude again in the red sample.

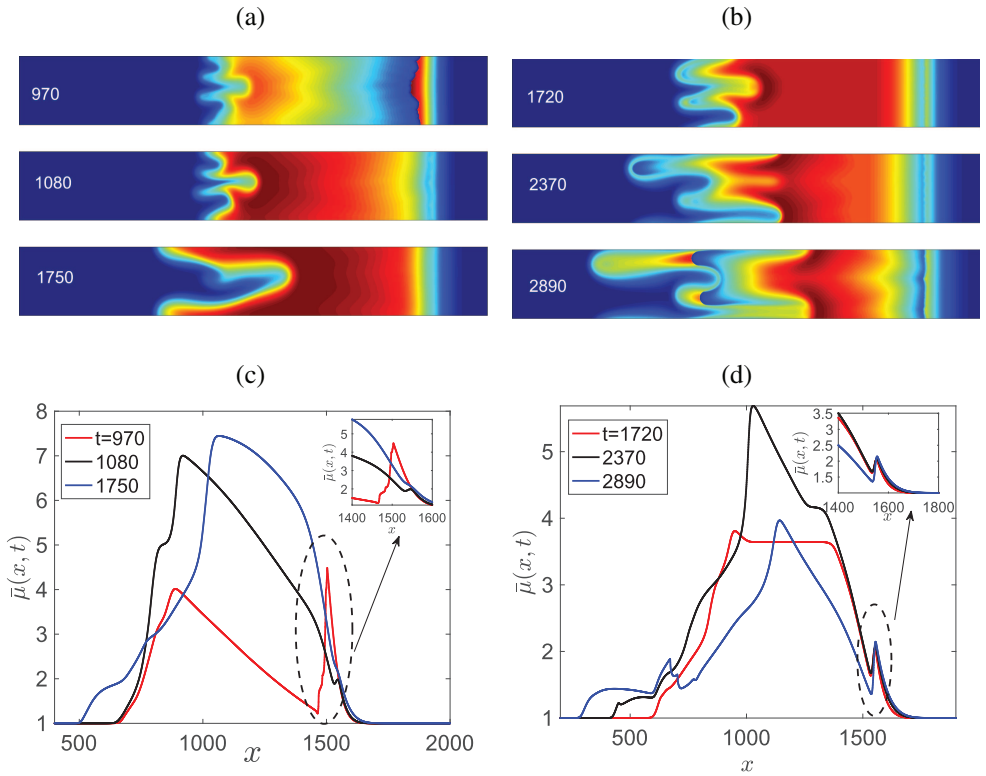

FIG. 11. Concentration fields of Y (top) showing additional viscous destabilization on the right part of the sample when a local nonmonotonic viscosity variation triggers VF and related viscosity profiles (bottom) at three different times for $R = 0.2$ and [(a) and (c)] $B_0 = 1$ and (b) $B_0 = 1.02$. The inset of the lower panels shows the local peaks in the viscosity responsible for the oscillation-driven fingering.

A summary of these dynamics in which subcritical oscillations are triggered by fingering is given by the space-time maps of Fig. 9, where the aperiodic oscillations due to the influence of VF can be seen. We appreciate that at $R = 0.15$, the system needs quite a long time for fingering to develop enough to fire the oscillation. At $R = 0.2$, oscillations are triggered earlier because fingering starts more rapidly. After three waves are triggered, a transient is needed for a new finger to build up and firing of oscillations to start again.

To understand the mechanism of the onset of the subcritical oscillations, we have to remind that diffusion of species occurs perpendicular to the interface between the two solutions. At the tip of a red, backward moving finger of the sample invading the blue A solution, the B, X, and Y species spread out radially such that, ahead of the finger, the reactant B and the intermediate species X and Y get more diluted than for a corresponding flat interface. The system is thus locally less able to oscillate. On the contrary, when B, X, and Y diffuse out of the sample in a valley of the red zone toward the tip of a blue finger protruding forward in the sample, they are more concentrated than in a planar case. Following scheme (1), the autocatalytic kinetics at the origin of the oscillatory bifurcation is therefore reinforced in the blue valleys where, locally, oscillations can be triggered for a value of B slightly lower than B_c.

Following this idea, we can anticipate that oscillations will be triggered earlier and at lower values of $B_0 < B_c$ if fingers of A extend more easily in the sample and if the curvature of a local finger is larger. This is possible if the system is more unstable toward fingering, i.e., if R increases. This is indeed what we observe, as seen in Fig. 10 where we plot the amplitude of the transversely averaged concentration $\bar{Y}(x_c, t)$ at the center position of the reaction zone as a function of B_0 for different values of R. From Fig. 10, we clearly see that VF is able to trigger subcritical oscillations in a zone of control parameter increasing when R increases.

D. VF induced by oscillations

The coupling between viscosity gradients and the oscillatory concentration dynamics of the intermediates can also induce a viscous destabilization of otherwise stable zones as seen in Fig. 11 from two examples: in the case of VF-induced subcritical oscillations for $B_0 < B_c$ [Figs. 11(a) and 11(c)] and for the oscillating VF when $B_0 > B_c$ [Figs. 11(b) and 11(d)]. At the left of the sample, we have the classical VF described above, due to the displacement of the more viscous sample by the less viscous solution of A ($R > 0$). However, the right part of the sample should be stable as, there, the more viscous sample is injected into the less viscous carrier fluid.[37] We observe nevertheless that, in the presence of oscillations of viscosity due to local oscillations of concentration, we can locally have tiny transverse modulations of this right stable zone. This is due to the presence in the oscillating traveling wave of local peaks of viscosity [see circled areas in Figs. 11(c) and 11(d)] in which a less viscous zone displaces a more viscous one, triggering VF locally in the right initially stable part of the sample thanks to the oscillations. As the concentration of Y is pulsating in the course of time [see Figs. 11(a) and 11(b)], so does the viscosity profile [Figs. 11(c) and 11(d)] in which some maxima form and vanish regularly, thus activating and suppressing successively the driving force for VF. As a consequence, convective fingers triggered by the oscillations form, grow, and fade away at irregular intervals. Note that, as fingering develops on the left and right part of the sample because of local adverse viscosity gradients that are not correlated, the respective oscillations are not necessarily in phase.

IV. CONCLUSION

We have numerically studied reaction-driven oscillating viscous fingering occurring when a viscous sample containing the reactants of the oscillatory Brusselator model is displaced by a less viscous solution of one of the reactants. Above the critical threshold for oscillations, the concentration of the intermediate species X and Y oscillates within the sample triggering oscillations of the viscosity of the solution varying with the concentration of Y. When oscillations interplay with viscous fingering, we find that fingering occurs earlier, with a smaller wavelength and is more intense with larger mixing zones than in the nonoscillating situation. This is due to the fact that oscillations of the concentration of Y trigger oscillations of viscosity and that, as a consequence, locally stronger viscosity gradients are experienced within the pulsatile viscosity field. This effect increases when the log-mobility ratio R controlling VF is increased. Viscous fingering can also influence the oscillations leading to a more rapid dilution and fading out of the oscillations because of more rapid convective mixing.

Most interestingly, the chemohydrodynamic coupling also induces new dynamic regimes that can only be obtained thanks to the interplay of chemistry and hydrodynamics. The first possibility is to obtain subcritical oscillatory behavior triggered by VF. We observe indeed that, when a finger of the solution of A protrudes within the sample rich in reactant B and intermediate species X and Y, a local oscillation can be triggered at the tip of the finger even if the initial concentration B_0 of the control parameter is smaller than its critical value to be reached to have oscillations in batch conditions. This is supposed to be due to the fact that the local curvature in the finger concentrates the concentration of species B, X, and Y locally such that an oscillation and a subsequent traveling wave can be triggered. The second possibility is that the oscillating dynamics is able to induce VF at the initially hydrodynamically stable interface where the more viscous sample pushes the less viscous solution of the reactant. This occurs thanks to the formation of nonmonotonic pulsatile viscosity profiles in which a local maximum can trigger the VF instability.

Our results evidence thus the rich wealth of possible new chemohydrodynamic behaviors that can be obtained thanks to the interplay between the symmetry-breaking properties of both hydrodynamic and chemical systems. From a theoretical point of view, a possible extension of the present work will include the study of the interplay of VF with Turing patterns using the model above when the X and Y intermediate species have different diffusion coefficients, along the line of what has already been done with buoyancy-driven convection.[18]

To search for experimental evidence of our predicted oscillating viscous fingering dynamics, the recent viscous fingering obtained using a clock reaction[26] with pH-changing properties[25] is a good starting point. The fact that front dynamics in $A + B \rightarrow$ oscillator configurations also start to be experimentally available in pH oscillators[23] enriches the possibility of trying to tune fingering using

pH-sensitive polymers.[10,11] It would be very nice to be able to couple viscous effects with the canonical oscillating Belousov–Zhabotinky reaction around an A + B → oscillator configuration.[17] While coupling of BZ localized oscillations in this configuration has already been done successfully for buoyancy-driven effects,[16,24] it still remains to see how to obtain large viscosity changes in the BZ system. We hope that the current work will trigger future efforts in this direction.

ACKNOWLEDGMENTS

C.R. and A.D.W. acknowledge the financial support of the FRS-FNRS PDR CONTROL program.

REFERENCES

[1] A. De Wit, Philos. Trans. R. Soc. A **374**, 20150419 (2016).
[2] R. Kapral and K. Showalter, *Chemical Waves and Patterns* (Springer, The Netherlands, 2012).
[3] I. R. Epstein and J. A. Pojman, *An Introduction to Nonlinear Chemical Dynamics: Oscillations, Waves, Patterns, and Chaos* (Oxford University Press, 1998).
[4] J. A. Pojman, I. R. Epstein, T. J. McManus, and K. Showalter, J. Phys. Chem. **95**, 1299 (1991).
[5] J. Masere, D. A. Vasquez, B. F. Edwards, J. W. Wilder, and K. Showalter, J. Phys. Chem. **98**, 6505 (1994).
[6] A. De Wit and G. M. Homsy, Phys. Fluids **11**, 949 (1999).
[7] L. Gálfi and Z. Rácz, Phys. Rev. A **38**, 3151 (1988).
[8] R. Tiani, A. De Wit, and L. Rongy, Adv. Colloid Interface Sci. **225**, 76 (2018).
[9] T. Podgorski, M. C. Sostarecz, S. Zorman, and A. Belmonte, Phys. Rev. E **79**, 016202 (2007).
[10] Y. Nagatsu, K. Matsuda, Y. Kato, and Y. Tada, J. Fluid Mech. **571**, 475 (2007).
[11] L. A. Riolfo, Y. Nagatsu, S. Iwata, R. Maes, P. M. J. Trevelyan, and A. De Wit, Phys. Rev. E **85**, 015304(R) (2012).
[12] T. Gérard and A. De Wit, Phys. Rev. E **79**, 016308 (2009).
[13] S. H. Hejazi, P. M. J. Trevelyan, J. Azaiez, and A. De Wit, J. Fluid Mech. **652**, 501 (2010).
[14] N. Sabet, H. Hassanzadeh, and J. Abedi, Phys. Rev. E **96**, 063114 (2017).
[15] N. Sabet, S. M. Jafari Raad, H. Hassanzadeh, and J. Abedi, Phys. Rev. Appl. **10**, 054033 (2018).
[16] D. M. Escala, J. Carballido-Landeira, A. De Wit, and A. P. Muñuzuri, J. Phys. Chem. Lett. **5**, 413 (2014).
[17] M. A. Budroni, L. Lemaigre, D. M. Escala, A. P. Muñuzuri, and A. De Wit, J. Phys. Chem. A **120**, 851–860 (2016).
[18] M. A. Budroni and A. De Wit, Chaos **27**, 104617 (2017).
[19] G. Nicolis and I. Prigogine, *Self-Organization in Nonequilibrium Systems* (Wiley, New York, 1977).
[20] A. M. Turing, Philos. Trans. R. Soc. B Biol. Sci. **237**, 37 (1952).
[21] V. Castets, E. Dulos, J. Boissonade, and P. De Kepper, Phys. Rev. Lett. **64**, 2953 (1990).
[22] M. A. Budroni and A. De Wit, Phys. Rev. E **93**, 062207 (2016).
[23] B. Dúzs and I. Szalai, Reac. Kinet. Mech. Cat. **123**, 335 (2018).
[24] L. Lemaigre, "Convective patterns triggered by chemical reactions, dissolution and cross-diffusion: An experimental study," Ph.D. thesis (Université libre de Bruxelles, 2016).
[25] D. M. Escala, A. P. Muñuzuri, A. De Wit, and J. Carballido-Landeira, Phys. Chem. Chem. Phys. **19**, 11914 (2017).
[26] D. M. Escala, A. De Wit, J. Carballido-Landeira, and A. P. Muñuzuri, Langmuir **35**(11), 4182–4188 (2019).
[27] I. Prigogine and R. Lefever, J. Chem. Phys. **48**, 1695 (1968).
[28] R. Lefever and G. Nicolis, J. Theor. Biol. **30**, 267 (1971).
[29] R. Lefever, G. Nicolis, and P. Borckmans, J. Chem. Soc. Faraday Trans. **84**, 1013 (1988).
[30] I. Prigogine and G. Nicolis, Q. Rev. Biophys. **4**, 107 (1971).
[31] M. Herschkowitz-Kaufman and G. Nicolis, J. Chem. Phys. **56**, 1890 (1972).
[32] J. Boissonade, J. Phys. France **49**, 541 (1988).
[33] G. Dewel and P. Borckmans, Phys. Lett. A **138**, 189 (1989).
[34] P. Borckmans, A. De Wit, and G. Dewel, Physica A **188**, 137–157 (1992).
[35] G. Dewel, P. Borckmans, A. De Wit, B. Rudovics, J.-J. Perraud, E. Dulos, J. Boissonade, and P. De Kepper, Physica A **213**, 181–198 (1995).
[36] A. De Wit, Y. Bertho, and M. Martin, Phys. Fluids **17**, 054114 (2005).
[37] M. Mishra, M. Martin, and A. De Wit, Phys. Rev. E **78**, 066306 (2008).
[38] D. Gottlieb and S. A. Orszag, *Numerical Analysis of Spectral Methods* (Society for Industrial and Applied Mathematics, 1989).
[39] C. T. Tan and G. M. Homsy, Phys. Fluids **31**, 1330 (1988).
[40] A. De Wit, Phys. Fluids **16**, 163 (2004).